Band nonparabolicity and three-dimensional aspects in quantum dots on InSb

P. Junker, U. Kops, and U. Merkt
Institut für Angewandte Physik, Universität Hamburg, Jungiusstrasse 11, 20355 Hamburg, Germany

T. Darnhofer and U. Rössler
Institut für Theoretische Physik, Universität Regensburg, 93040 Regensburg, Germany
(Received 20 September 1993)

Quantum dots with high lateral quantization energies are created on InSb by means of a perforated Schottky gate. With a gate voltage the lateral quantization energies can be tuned and approach values up to $\hbar\omega_0 \approx 25$ meV, which is comparable to the subband separations connected with the vertical motion in the corresponding quasi-two-dimensional electron system. By far-infrared spectroscopy, we observe the two fundamental modes $\omega_\pm$ in a magnetic field and verify the predicted polarization selection rules. The measured transition energies are described by employing a realistic three-dimensional model potential and taking into account the conduction band nonparabolicity of InSb and the resulting coupling of the vertical subbands.

INTRODUCTION

Quantum dots in semiconductors originate from the confinement of quasi-two-dimensional electron gases in both lateral dimensions on the length scale of the de Broglie wavelength. This way, one creates totally quantized, atomiclike electron systems.[1–4] Unlike in donors or real atoms with their Coulomb potentials, the external potential for the electrons in a quantum dot is not well defined. It depends on the position and number of fixed charges on surface states, donors, or acceptors, and on the metal gates, which are, in general, only poorly known.[5] For these reasons, a parabolic lateral confinement potential $\frac{1}{2}m^*\omega_0^2\varrho^2$ with a phenomenological frequency ω_0 and the effective-mass-approximation (EMA) with an effective electron mass m^* has often been used as a first approximation to describe the two observed far-infrared (FIR) modes $\omega_\pm$.[1] The success of this simple model is based on a generalization of Kohn's theorem,[6] which states that the intrinsic many-particle character of such dots cannot be seen in the dipole spectra, as the dipole operator couples only to the center-of-mass motion.[7–9]

In our quantum dot samples, lateral quantization energies up to $\hbar\omega_0 \approx 25$ meV are achieved. In particular, these high quantization energies allow the verification of the theoretically predicted polarization selection rules of the fundamental modes $\omega_\pm$ in magnetic fields at convenient wavelengths $\lambda \approx 100$ μm in the FIR regime.

Suggested by the geometry of our samples, we introduce a three-dimensional confinement potential which is derived from the simple electrostatic model of a conducting plane with a circular hole in it.[10] Taking into account the nonparabolicity of the InSb conduction band as well as the resulting coupling of the lateral and vertical motion of the dot electrons, we obtain a qualitative description of the experimentally observed transition energies.

I. EXPERIMENTAL DETAILS

The idea of the InSb quantum dots is sketched in Fig. 1(a). Essentially, we have a metal-oxide-semiconductor structure with the alloy NiCr on the InSb as a perforated

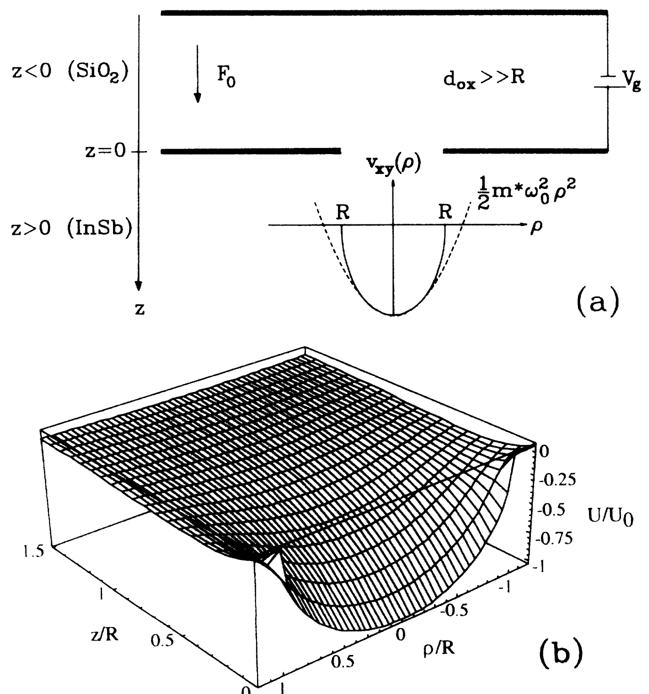

FIG. 1. (a) Sketch of the quantum dot structure and of the resulting lateral potential at the interface ($z = 0$). (b) Electrostatic potential $U(\mathbf{r})$ given by Eq. (2) for the model of a conducting plane with a circular hole of radius R, plotted in units of its depth $U_0 = eF_0R/\pi$ as a function of the dimensionless cylindrical coordinates ϱ/R and z/R.

 ©1994 The American Physical Society

Schottky barrier.[11] This pins the Fermi energy at the NiCr-InSb interface above the valence band edge. Underneath the narrow regions between the NiCr mesh, mobile inversion electrons are induced by the gate voltage V_g. The resulting lateral potential at the InSb surface ($z = 0$) is also sketched in Fig. 1(a). For intensity reasons we must fabricate about 10^8 dots on a single sample. There is virtually no tunneling between adjacent dots since the barrier height between dots is of the order of the band-gap energy $E_g = 236$ meV and the distance is comparable to the grating constant $a = 400$ nm of the quadratic dot array. Also, the FIR resonance frequencies are virtually unaffected by electromagnetic coupling between individual dots.[9]

The samples are fabricated by holographic lithography, NiCr shadowing, and liftoff of the photoresist in acetone. The later preparation step creates the holes in the NiCr Schottky barrier with typical radii $R \approx 150$ nm. Finally, a SiO_2 gate insulator is deposited by plasma-enhanced chemical vapor deposition and the homogeneous NiCr top gate is evaporated.[12,13] Via field effect, the dots can be charged without having a contact layer, since the InSb substrate has a finite resistivity in the megaohm regime even at liquid helium temperatures. We determine the threshold voltage V_t from the onset of absorption and establish a certain number n_0 of electrons in an individual dot by the voltage difference $\Delta V_g = V_g - V_t$.

The spectra are taken at liquid helium temperature $T \approx 2$ K for various lines of a FIR waveguide laser. In some experiments the radiation is circularly polarized with the aid of a wire-grid polarizer and quarter-wave plates made from y-cut quartz crystals of appropriate thicknesses. We record the relative change in transmittance $\Delta T/T = [T(V_t) - T(V_g)]/T(V_t) \ll 1$ versus the strength B of a magnetic field which is applied perpendicular to the dots. This signal is related to the high-frequency conductivity $\sigma(\omega, B)$ of the dot electrons by the Fresnel formula

$$\frac{\Delta T}{T} = \frac{2}{a^2} \frac{\sigma(\omega, B)/Y_0}{1 + \sqrt{\varepsilon} + \sigma_\square/Y_0} \tag{1}$$

with the vacuum admittance $Y_0 = 1/(\mu_0 c)$, the grating constant a, the dielectric constant ε of the semiconductor, and the total sheet resistivity $\sigma_\square$ of the metallizations.

II. THEORY

A. Model potential

To describe the confinement of the electrons in our quantum dot structure, we start from the simple electrostatic model of a conducting sheet in the xy plane with a circular hole of radius R, and an applied electric field in the half space $z < 0$ which is constant $\mathbf{F}_0 = (0, 0, F_0)$ far away from the hole. For an idealized structure without charged interface states and with no discontinuity in the dielectric constants of oxide and semiconductor, the field strength $F_0 = V_g/d_{\text{ox}}$ would be determined by the gate voltage V_g and the oxide thickness d_{ox}. In cylindrical coordinates (ϱ, φ, z), the electrostatic potential of this configuration for $z > 0$ is given by[10]

$$U(\mathbf{r}) = -\frac{eF_0 R^2}{\pi} \int_0^\infty dk\, j_1(kR)\, e^{-kz} J_0(k\varrho) \,. \tag{2}$$

Numerically determined values for $U(\mathbf{r})$ are shown in Fig. 1(b) as a function of ϱ and z. Close to the center of the hole, this potential can be approximated by its expansion for $\varrho \ll R$,

$$U(\mathbf{r}) \approx -\frac{eF_0 R}{\pi} + \frac{eF_0}{\pi} z \arctan\left(\frac{R}{z}\right) + \frac{eF_0}{2\pi R} \left[1 + \left(\frac{z}{R}\right)^2\right]^{-2} \varrho^2 \,. \tag{3}$$

The first term $U_0 = -eF_0 R/\pi$ is a constant energy shift describing the depth of the dot potential. The derivative of the second term is an electric field in the z direction independent of ϱ. The presence of charged interface states and the discontinuous change of the dielectric constant from the oxide to the semiconductor will change this electric field inside the semiconductor. For the sake of simplicity, we describe the resulting vertical, z-dependent part of the potential within the common triangular-well approximation[14,15]

$$v_z(z) = \begin{cases} \infty & z < 0 \\ eFz & z > 0 \,, \end{cases} \tag{4}$$

and choose the total field F as an adjustable parameter. The third term in (3) is a parabolic lateral confinement with a curvature that decreases with increasing distance away from the interface. Motivated by these considerations, we use the model potential

$$V(\mathbf{r}) = v_z(z) + v_{xy}(\varrho) + \left\{\left[1 + \left(\frac{z}{R}\right)^2\right]^{-2} - 1\right\} v_{xy}(\varrho) \,, \tag{5}$$

where $v_z(z)$ is the triangular potential given by (4), and $v_{xy}(\varrho) = \frac{1}{2} m^* {\omega_0}^2 \varrho^2$ is the common parabolic lateral confinement. The last term in (5) cannot be separated and leads to a coupling of the electron motion in the z direction to the motion in the xy plane in this three-dimensional potential.

B. Kinetic energy

To consider the nonparabolicity in the conduction band of a semiconductor with fundamental gap E_g and effective mass m^*, we start from the kinetic energy term[16]

$$\frac{E_g}{E_g + E - V(\mathbf{r})} \frac{p^2}{2m^*} \approx \frac{p^2}{2m^*} + \left(\frac{E_g}{E_g + E - V(\mathbf{r})} - 1\right) [E - V(\mathbf{r})] \,, \tag{6}$$

where E is the eigenenergy of the Hamiltonian with the confinement potential $V(\mathbf{r})$. In (6) we used the approximative replacement $p^2/2m^* \approx E - V(\mathbf{r})$ to obtain the sum of the kinetic energy in EMA and a correction. This replacement and the Taylor expansion for $E-V(\mathbf{r}) \ll E_g$ leads to a simpler correction proportional to p^4, which is equal to a sum of terms for the z direction, for the xy plane, and a coupling term:

$$-\frac{1}{E_g}\left(\frac{p^2}{2m^*}\right)^2 = -\frac{1}{E_g}\left(\frac{p_z^2}{2m^*}\right)^2 - \frac{1}{E_g}\left(\frac{p_x^2+p_y^2}{2m^*}\right)^2 - \frac{2}{E_g}\frac{p_x^2+p_y^2}{2m^*}\frac{p_z^2}{2m^*} . \quad (7)$$

We include a magnetic field in the z direction by adding the vector potential to the components p_x and p_y. As a consequence, the second term on the right-hand side of (7) contains a part proportional to B^4 that would strongly overestimate the nonparabolicity for higher magnetic fields. Therefore, we make the approximative replacement and the definition

$$-\frac{1}{E_g}\left(\frac{p_x^2+p_y^2}{2m^*}\right)^2 \approx \left(\frac{E_g}{E_g+E_{xy}-v_{xy}(\varrho)}-1\right) \times[E_{xy}-v_{xy}(\varrho)] =: K(\varrho) , \quad (8)$$

where we compared (7) with (6), and assumed a nearly separable potential, which allows us to introduce the eigenenergy E_{xy} for the xy plane. The motion in the z direction is not affected by the magnetic field, so that the term proportional to p_z^4 will always be small and can be neglected in our simple description of the subband problem by the triangular-well potential (4) with the field F as an adjustable parameter. With these approximations, we get a kinetic energy term that consists of a separable part and a coupling term:

$$\frac{E_g}{E_g+E-V(\mathbf{r})}\frac{p^2}{2m^*} \approx \frac{p_z^2}{2m^*} + \frac{p_x^2+p_y^2}{2m^*} + K(\varrho) - 2\frac{p_z^2}{2m^*}\sqrt{\frac{-K(\varrho)}{E_g}} . \quad (9)$$

C. Subband coupling

Let us first consider the problem without the nonparabolicity correction $K(\varrho)$ and without the coupling between motions in the z direction and xy plane. In this case the problem separates into the Schrödinger equation for the z direction with the triangular potential (4) and the two-dimensional harmonic oscillator in a magnetic field. The solutions of the former, the subband functions $\langle z|j\rangle = \xi_j(z)$ and eigenenergies $E_z(j)$ for $j = 1,2,...$, are given analytically in terms of the Airy function and its zeros.[14,15] Due to the axial symmetry, the eigenfunctions of the oscillator can be written as $\langle x,y|n,m\rangle = R_{n|m|}(\varrho)\, e^{im\varphi}$, for the angular momentum $m = 0,\pm1,\pm2,...$ and the radial quantum number $n = 0,1,2,...$. In terms of the cyclotron frequency $\omega_c = eB/m^*$ and the hybrid frequency $\omega = \sqrt{\omega_c^2/4+\omega_0{}^2}$, the eigenenergies are given by[17,18]

$$E_{xy}(n,m) = (2n+|m|+1)\hbar\omega + \frac{\hbar\omega_c}{2}m . \quad (10)$$

With the selection rule $\Delta m = \pm1$, this system exhibits two allowed dipole transitions with the energies

$$\Delta E_\pm = \hbar(\omega \pm \omega_c/2) = \hbar\omega_\pm . \quad (11)$$

For zero magnetic field, this gives $\hbar\omega_\pm = \hbar\omega_0$. This transition energy is split in a magnetic field, and with increasing field the ω_+ mode approaches the cyclotron resonance ω_c, while the ω_- mode goes to zero.

The correction to the kinetic energy $K(\varrho)$ given by (8) is an axially symmetric function of ϱ, depending on the energy $E_{xy}(n,m)$ given by (10). It is diagonal in m and couples only states with different n, which are separated by an energy of at least $2\hbar\omega$. Therefore, the mixing of states induced by this term is negligible and it suffices to consider $K(\varrho)$ in first order perturbation theory. The corresponding integrals $K_{nm} = \langle n,m|K|n,m\rangle$ with the radial functions $R_{n|m|}(\varrho)$ have to be determined numerically. This correction lowers all eigenenergies by amounts that are bigger for higher levels and increase with magnetic field strength. Therefore the ω_+ mode is shifted to lower frequencies compared to the EMA results given by (11).[16]

Without subband coupling, the eigenenergies of the system are given by $E(j;n,m) = E_z(j) + E_{xy}(n,m) + K_{nm}$ and the eigenfunctions are products $|j\rangle \otimes |n,m\rangle$. These states are coupled by the two terms

$$\frac{1}{2}m^*\omega_0^2\varrho^2\left\{\left[1+\left(\frac{z}{R}\right)^2\right]^{-2}-1\right\} - 2\frac{p_z^2}{2m^*}\sqrt{\frac{-K(\varrho)}{E_g}} , \quad (12)$$

which arise from the nonseparability of the model potential (5) and the kinetic energy (9), respectively. We consider this coupling by a numerical diagonalization of the corresponding matrix for a finite number of subbands. For the results shown below, we included the five lowest vertical subbands $j = 1,2,...,5$. As in the case for $K(\varrho)$, this coupling is diagonal in m, and coupling of states with different n can be neglected. The matrix elements $\langle j|[1+(z/R)^2]^{-2}|j'\rangle$, $\langle j|p_z^2|j'\rangle$ and the integrals $\langle n,m|\sqrt{-K(\varrho)}|n,m\rangle$ have to be determined numerically, but we can use an analytical expression for $\langle n,m|\varrho^2|n,m\rangle$. We denote the new eigenenergies and corresponding eigenstates that result from the diagonalization by $\tilde{E}(\tilde{j};n,m)$ and $|\tilde{j};n,m\rangle$. The new quantum number $\tilde{j}$ arises from subband mixing, while m remains a good quantum numbers because of the axial symmetry and the mixing in n is neglected in our approximations.

III. EXPERIMENTAL RESULTS

The spectra in Fig. 2 are obtained for a sample with grating constant $a = 400$ nm of the quadratic dot array

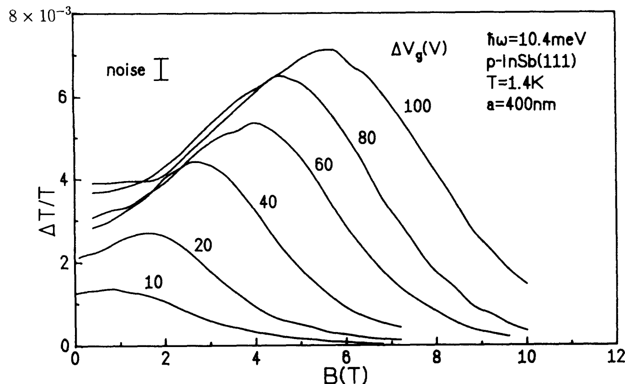

FIG. 2. FIR laser spectra of a quantum dot sample. The relative change in transmittance $-\Delta T/T$ vs magnetic field strength is shown for different gate voltages ΔV_g above threshold.

and a geometrical radius $R \approx 180$ nm of an individual dot was estimated from micrographs of samples processed in the same run. With increasing gate voltages the resonance position shifts to higher magnetic field strengths which is characteristic for the ω_- mode according to (11) when the quantization energy $\hbar\omega_0$ increases. The integrated signal strength is found to increase in proportion to the gate voltage above threshold and there is no saturation in the number of electrons. Instead, the electron number n_0 is only limited by the breakdown voltage of the gate oxide.[19] In this particular sample, we observe a threshold voltage $V_t = 20$ V and a linear increase of the electron number $n_0/\Delta V_g = (6.7 \pm 0.1)$ V^{-1}.

We have verified the polarization selection rules with the aid of wire-grid polarizers and quarter-wave plates made from y-cut quartz of appropriate thickness. In these experiments the degree of circular polarization was limited to about 80% of its ideal value presumably due to cavity effects in our sample holder.[20] For comparative reasons, the two spectra in Fig. 3(a) were recorded for a homogeneous two-dimensional electron gas on InSb ($n_s \approx 10^{12}$ cm^{-2}, $m^* = 0.023\ m_e$) for the cyclotron resonance active B^+ and inactive B^- direction of the magnetic field, respectively. Spectra for a dot sample are given in Fig. 3(b). Predominantly, the ω_+ and ω_- modes are excited in the B^+ and B^- configuration, respectively. This agrees with the theoretical selection rules underlying (11).[13]

The observed resonance energies versus magnetic field strength are shown in Fig. 4 for three particular gate voltages. The dashed lines represent the result in EMA according to (11) using the effective mass $m^* = 0.0135 m_e$ for InSb and treating the quantization energy $\hbar\omega_0$ as an adjustable parameter. Within this model it is not possible to describe the observed resonance positions satisfactorily. For all quantization energies $\hbar\omega_0$, the ω_+ and ω_- modes given by (11) lie systematically higher and lower, respectively, than the measured resonance energies. The solid lines that result from our theory provide a significantly better description.

IV. DISCUSSION

The form of our model potential (5) and the kinetic energy (9) do not allow a strict application of Kohn's theorem: the center-of-mass motion of the many-particle system is coupled to the relative motion by nonparabolicities in the energy-momentum relation and the potential. However, this coupling is so weak that the resulting deviations from a simple two-mode spectrum or other many-particle effects cannot be resolved in our experiments. Therefore, we can still describe the observed resonance positions by the dipole transitions between different center-of-mass states which can be given by our calculations in Sec. II. We consider the transitions from the ground state, whose energy differences are $\Delta\tilde{E}_\pm = \tilde{E}(1;0,\pm1) - \tilde{E}(1;0,0)$. The solid lines in Fig. 4 show plots of $\Delta\tilde{E}_\pm$ versus the magnetic field strength. Due to subband coupling, the transition energies at zero field $\hbar\tilde{\omega}_0 = \Delta\tilde{E}_\pm(B = 0)$ are always smaller than the

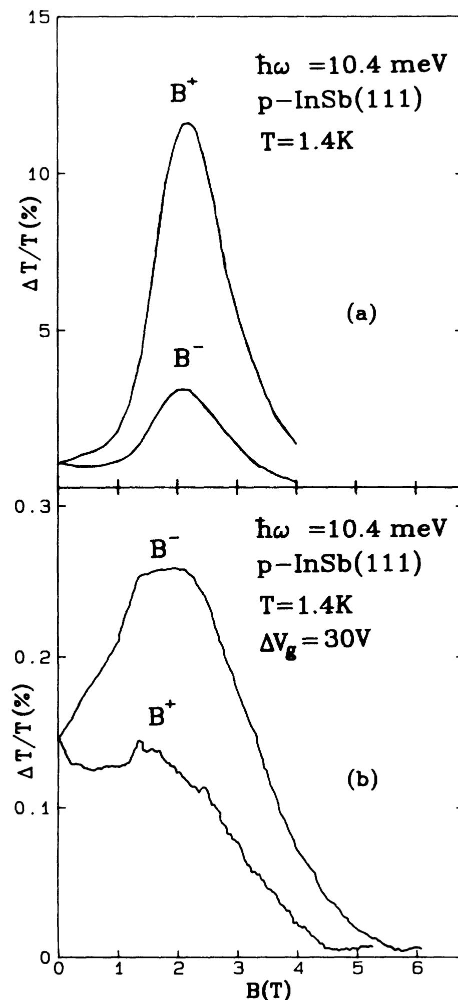

FIG. 3. (a) Cyclotron resonance of a homogeneous two-dimensional electron gas on InSb for the cyclotron resonance active B^+ and inactive B^- direction of the magnetic field. (b) Corresponding spectra for a quantum dot sample, demonstrating the polarization selection rule of the ω_- mode.

bare oscillator energies $\hbar\omega_0$, which are marked by arrows on the vertical axes in Fig. 4. As the magnetic field dependence of $\Delta\tilde{E}_\pm$ is determined by the ratio $\hbar\omega_c/\hbar\omega_0$, they lie at higher fields than the transition energies $\Delta E_\pm$ of a simple harmonic oscillator with frequency $\tilde{\omega}_0$, which are shown in Fig. 4 by dotted lines and whose field dependence is determined by $\hbar\omega_c/\hbar\tilde{\omega}_0$. As a consequence, the ω_- mode is shifted to higher energies, while the ω_+ mode is lowered. This tendency can clearly be seen in the observed resonance positions in Fig. 4.

To fit the calculated transition energies $\Delta\tilde{E}_\pm$ to the experimental data for the gate voltages V_g = 30, 60, 80, 100, and 120 V, we can vary the two parameters F and $\hbar\omega_0$ of our model potential (5). For the hole radius we use $R = 180$ nm. We get good agreement by choosing F proportional to the gate voltage V_g as shown in Fig. 5(a). The onset of -50 V differs from the threshold voltage $V_t = +20$ V, which can be explained qualitatively by the intrinsic field of the oxide-semiconductor interface: to achieve $F = 0$, which is the flat band condition at the interface, it would be necessary to apply a negative gate voltage of $V_g = -50$ V, whereas the first dot electrons are only induced at $V_g = V_t = +20$ V. The chosen values of F ranging from 1.2 to 2.5×10^{-4} eV/Å lead to subband separations $E_z(2) - E_z(1)$ from 28 to 46 meV, which is, in fact, what one observes in comparable quasi-two-dimensional systems.[21]

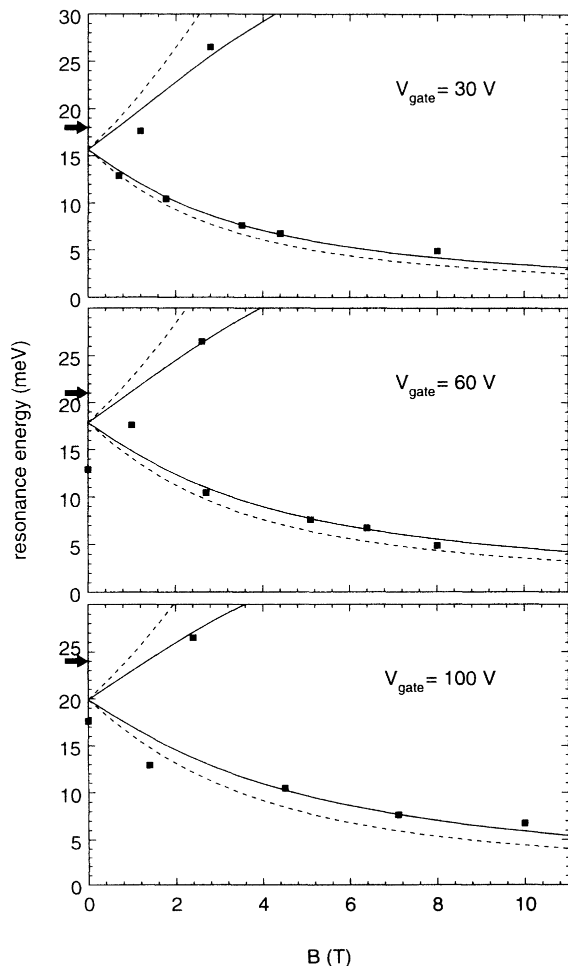

FIG. 4. Experimental resonance positions $\hbar\omega_\pm$ as a function of the magnetic field strength for three particular gate voltages in comparison with the theoretical values in EMA given by Eq. (11) (dotted lines) and the theoretical transition energies $\Delta\tilde{E}_\pm$ from the present work (solid lines). The quantization energies $\hbar\omega_0$ used in the present theory are marked by arrows on the vertical axes.

Best values for $\hbar\omega_0$ are plotted in Fig. 5(b) versus the gate voltage. The Schottky contact at the metal-semiconductor interface outside the hole ($\varrho > R$) results in an almost flat conduction band.[11] For $V_g = -50$ V we assumed also a vanishing vertical electric field $F = 0$ inside the hole, so that we expect a flat lateral potential $\hbar\omega_0 = 0$ for this gate voltage. The increment of $\hbar\omega_0$ with increasing gate voltage can be fitted by a square root dependence, which is shown in Fig. 5(b) by the dotted line. This behavior can be understood if we compare the prefactor of the parabolic lateral potential which is proportional to ω_0^2 with the prefactor of the term proportional to ϱ^2 in (3) which is proportional to F_0. Since the electric field is proportional to the gate voltage above flat-band condition, we get $\hbar\omega_0$ proportional to $\sqrt{V_g + 50\ \text{V}}$. The prefactor of this proportionality, and the offset of -50 V cannot be explained by our simple electrostatic model, as it does not include the modifications due to the effects of the oxide-semiconductor interface and the difference between the dielectric constants of InSb and SiO_2.

To evaluate the mutual importance of band nonparabolicity and three-dimensionality of the confinement potential, we repeated our computations considering only one of the two coupling terms given by (12). For InSb

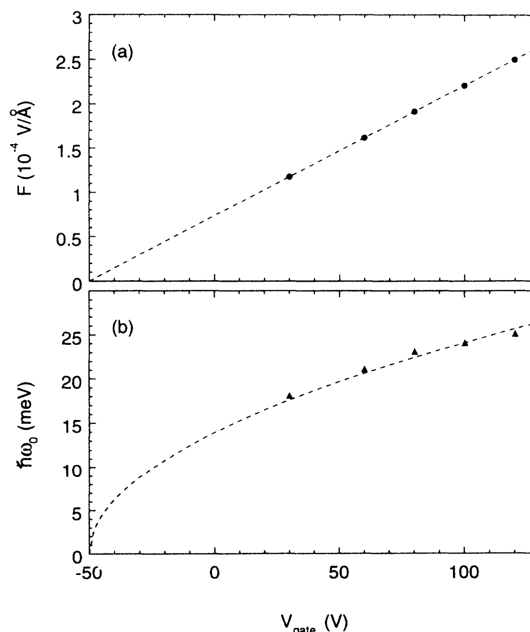

FIG. 5. Strengths F of the vertical electric field (a) and lateral quantization energies $\hbar\omega_0$ (b) as used in the description of the experimental data in Fig. 4. The expected linear and square-root dependence on the applied gate voltage V_g is indicated by the dotted lines.

parameters the coupling due to the kinetic energy has a stronger influence, but both terms induce energy changes with the same tendency and of the same order. Only for quantum dots on InSb with a low lateral quantization energy of $\hbar\omega_0 = 7.5$ meV,[1] which is much smaller than the separation of the vertical subbands, the subband coupling is negligible and the transition energies can be determined within a two-dimensional model. The influence of band nonparabolicity, however, remains important.[16]

SUMMARY AND CONCLUSION

We present an improved scheme for the fabrication of quantum dots on InSb, allowing high lateral quantization energies $\hbar\omega_0$ comparable to the spacings of quasi-two-dimensional subbands in the corresponding homogeneous system. This is mainly due to the small effective electron mass in this narrow-gap semiconductor and makes two new demands on a successful theoretical description. First, one has to take into account the band structure of the semiconductor beyond EMA, specifically, the nonparabolicity of the conduction band.[16] Second, the problem can no longer be treated within a two-dimensional model, since the coupling of horizontal and vertical motion becomes important.

The present theory provides a realistic description of the experimental FIR resonance positions despite its neglect of many-particle effects. In principle, band nonparabolicity violates the preconditions for the generalized Kohn theorem and the spectra should be modified.[16,22] However, in the present experiments we only observe resonances of the center-of-mass motion exhibiting to a large extent positions and selection rules already predicted by the EMA. This is due to the polarization direction of the incident radiation, the still relatively weak coupling of the lateral and vertical motion, and the broad width of the resonances, that prevent the observation of spectral details. Specific line splittings, caused by the coupling of relative and center-of-mass motion and spin-orbit coupling, have been predicted for narrow-gap semiconductors,[16] but are too small to be resolved in our experiments. In GaAs quantum dots with their much sharper lines other features have been observed.[2,4] Many-particle effects due to a nonparabolic two-dimensional confinement potential give theoretical explanations for these experimental results.[23,24]

We would like to add here that large quantization energies in quantum dots offer far-reaching physical possibilities such as, for example, the study of the long known polaron problem[25] with few or many quasiparticles, when the quantization energies reach the LO-phonon energies of the semiconductor, as is already the case for InSb. A reliable evaluation of this effect, however, requires understanding of the electronic dot structure including a more precise description of the external potential and the impact of the band structure. We consider the present work as a step in this direction.

ACKNOWLEDGMENT

This work was performed with financial support from the Deutsche Forschungsgemeinschaft within the SFB 348 in Regensburg and the project 916/4 in Hamburg.

[1] Ch. Sikorski and U. Merkt, Phys. Rev. Lett. **62**, 2164 (1989).
[2] T. Demel, D. Heitmann, P. Grambow, and K. Ploog, Phys. Rev. Lett. **64**, 788 (1990).
[3] A. Lorke, J. P. Kotthaus, and K. Ploog, Phys. Rev. Lett. **64**, 2559 (1990).
[4] B. Meurer, D. Heitmann, and K. Ploog, Phys. Rev. Lett. **68**, 1371 (1992).
[5] A. Kumar, S. E. Laux, and F. Stern, Phys. Rev. B **42**, 5166 (1990).
[6] W. Kohn, Phys. Rev. **123**, 1242 (1961).
[7] P. A. Maksym and T. Chakraborty, Phys. Rev. Lett. **65**, 108 (1990).
[8] L. Brey, N. F. Johnson, and B. I. Halperin, Phys. Rev. B **40**, 10 647 (1989).
[9] P. Bakshi, D. A. Broido, and K. Kempa, Phys. Rev. B **42**, 7416 (1990).
[10] D. Jackson, *Classical Electrodynamics* (Wiley, New York, 1962), Sec. 3.13.
[11] Ch. Sikorski, J. Vac. Sci. Technol. B **8**, 625 (1990).
[12] U. Mackens and U. Merkt, Thin Solid Films **97**, 53 (1982).
[13] U. Merkt, Ch. Sikorski, and J. Alsmeier, in *Spectroscopy of Semiconductor Microstructures,* edited by G. Fasol, A. Fasolino, and P. Lugli (Plenum, New York, 1989), p. 89.
[14] F. Stern, Phys. Rev. B **5**, 4891 (1972).
[15] T. Ando, A. B. Fowler, and F. Stern, Rev. Mod. Phys. **54**, 437 (1982).
[16] T. Darnhofer and U. Rössler, Phys. Rev. B **47**, 16 020 (1993).
[17] V. Fock, Z. Phys. **47**, 446 (1928).
[18] C. G. Darwin, Proc. Cambridge Philos. Soc. **27**, 86 (1931).
[19] U. Merkt, Physica B **189**, 165 (1993).
[20] U. Kops, diploma thesis, Universität Hamburg, 1992.
[21] W. Beinvogl and J. F. Koch, Solid State Commun. **24**, 687 (1977).
[22] U. Rössler, D. A. Broido, and F. Bolton, in *Low Dimensional Electronic Systems*, edited by F. Kuchar, G. Bauer, and H. Heinrich, Springer Series in Solid State Sciences Vol. 111 (Springer, Berlin, 1992), p. 21.
[23] V. Gudmundsson and R. Gerhardts, Phys. Rev. B **43**, 12 098 (1991).
[24] D. Pfannkuche and R. Gerhardts, Phys. Rev. B **44**, 13 132 (1991).
[25] T. Devreese, Phys. Scr. T **25**, 309 (1989).